Surface-to-Surface Transition via Electromagnetic Coupling of Microstrip and Coplanar Waveguide

JOHN J. BURKE, STUDENT MEMBER, IEEE, AND ROBERT W. JACKSON, SENIOR MEMBER, IEEE

Abstract—**A structure is described which forms a transition from coplanar waveguide on one substrate to microstrip on another. Energy is transferred via electromagnetic coupling rather than with wire bonds. A full-wave formulation along with the theory of asymmetrically coupled lines is used to analyze the transition. Two model transitions were built and tested. Theory and measurement show good agreement when the coupler length to width ratio is larger than 0.6.**

I. Introduction

WIRE BONDING is currently the method most often used to connect one microwave module (GaAs chip, hybrid printed antenna) to another. At millimeter-wave frequencies, wire bonding can seriously degrade circuit operation and is very labor intensive. In large phased array antenna systems with tens of thousands of elements, elimination of critical wire bonds is likely to improve performance and reduce cost [1].

This paper describes a method of coupling from a coplanar waveguide transmission line on one substrate surface (possibly a motherboard) to a microstrip transmission line on another (an MMIC or hybrid circuit). Coupling is achieved electromagnetically and no wire bonds are necessary. Fig. 1 shows the configuration in which a "chip" substrate having microstrip circuitry is connected to a coplanar waveguide feed line on a "motherboard" substrate by merely placing one substrate on top of the other. The ground plane of the "chip" is removed in the area over the coupling region. Elsewhere, the chip and motherboard ground planes coincide. A related structure has been described previously in which a coplanar waveguide "chip" was coupled to a coplanar waveguide motherboard [2]. Since microstrip is a widely used circuit medium, the transition described in this work should be of interest to workers in the MIC field.

In what follows, the transition is modeled as a set of coupled lines with two of the four possible ports terminated in open circuits. These lines are asymmetrically coupled to each other and therefore require a more complicated analysis than the symmetric coupler previously described in [2]. A coupled line full-wave analysis is very briefly outlined in the following section, with special note made of the various impedance definitions necessary. Section III describes experimental models which were built and tested. The effects of substrate characteristics and discontinuities are described in Section IV.

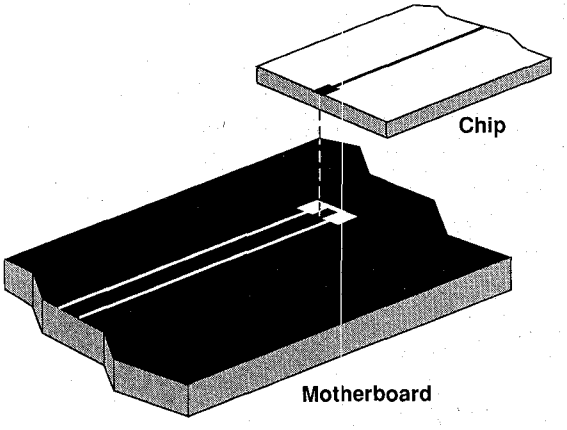

Fig. 1. Schematic drawing of CPW motherboard and electromagnetically coupled microstrip chip.

II. Analysis

The structure shown in Fig. 1 consists of a four-port coupled line section with one port connected to an input line on one surface, one port connected to an output line on the other surface, and the remaining ports terminated in open circuits. Fig. 2 shows a cross section of the coupling region assuming no motherboard is present. Since there is no up–down symmetry inherent in this problem, asymmetric coupled line analysis [3] must be used. Also, the cross-sectional size of the structure is a significant fraction of a wavelength and therefore the propagation constants and impedances should be determined using a full-wave analysis.

A. Asymmetric Coupled Line Analysis

Fig. 2 shows the current configurations for the two asymmetric modes which are used in the analysis of this coupler. It should be noted that for the π mode, the total current on either side conductor is at least an order of magnitude smaller than the total current on the center

Manuscript received December 28, 1987; revised August 12, 1988. This work was supported in part by the Electronics Laboratory, General Electric Company, Syracuse, NY.

The authors are with the Department of Electrical and Computer Engineering, University of Massachusetts, Amherst, MA 01003.

IEEE Log Number 8825376.

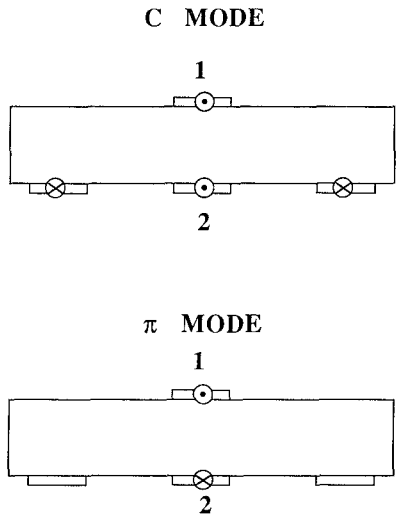

Fig. 2. Schematic of current configurations for each mode.

conductor. It is for this reason that no direction is indicated for the π mode side conductor current. Using quasi-static assumptions, Tripathi [3] has derived an impedance matrix which can be applied to this problem (two of the possible four ports are open-circuited):

$$\begin{bmatrix} Z_{11} & Z_{13} \\ Z_{31} & Z_{33} \end{bmatrix} = -j\frac{Z_{c1}}{1-K_\pi/K_c}\begin{bmatrix} \cot\beta_c L & -K_\pi \csc\beta_c L \\ -K_\pi \csc\beta_c L & K_\pi^2 \cot\beta_c L \end{bmatrix} - j\frac{Z_{\pi 1}}{1-K_c/K_\pi}\begin{bmatrix} \cot\beta_\pi L & -K_c \csc\beta_\pi L \\ -K_c \csc\beta_\pi L & K_c^2 \cot\beta_\pi L \end{bmatrix} \quad (1)$$

where

$$Z_{cj} = \frac{V_{cj}}{I_{cj}} \quad (2a)$$

$$Z_{\pi j} = \frac{V_{\pi j}}{I_{\pi j}}, \qquad j = 1 \text{ or } 2 \quad (2b)$$

$$K_c = \frac{I_{c1}}{I_{c2}} \quad (3a)$$

$$K_\pi = \frac{I_{\pi 1}}{I_{\pi 2}} \quad (3b)$$

$$\frac{Z_{c2}}{Z_{c1}} = \frac{Z_{\pi 2}}{Z_{\pi 1}} = -K_c K_\pi. \quad (4)$$

The c and π subscripts refer to the two modes illustrated in Fig. 2. The currents I_{c1} (I_{c2}) and $I_{\pi 1}$ ($I_{\pi 2}$) refer to the total longitudinal currents of the c and π modes on the conductor labeled 1 (2) in Fig. 2. The voltages V_{c1} (V_{c2}) and $V_{\pi 1}$ ($V_{\pi 2}$) refer to the potentials of the c and π modes on the conductor labeled 1 (2) referenced to the side conductor potential. The constants K_c and K_π defined here are equal to $-R_\pi$ and $-R_c$, defined in [3]. For a quasi-static case, the impedances Z_{c1}, Z_{c2}, $Z_{\pi 1}$, and $Z_{\pi 2}$ are uniquely defined by (2). In the full-wave case, these impedances are not uniquely defined, and modifications must be made in order to ensure power conservation. These modifications will be discussed in the next section.

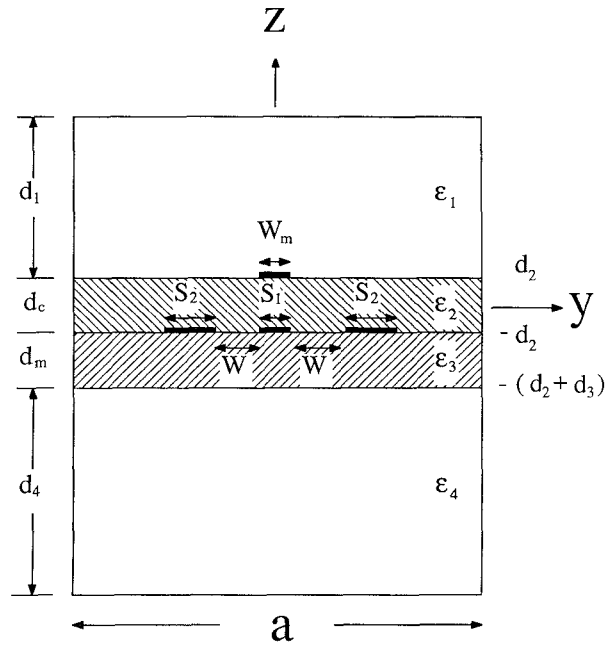

Fig. 3. Configuration used in the analysis of the microstrip CPW coupler.

B. Full-Wave Analysis

Fig. 3 shows the geometry of the microstrip CPW coupler in a perfectly conducting box. The sidewalls of the box are set far enough away to have a negligible effect on the modes of interest. Enclosing the structure introduces one additional mode, but this mode has no effect on the physical structure which is to be analyzed and is therefore neglected.

Since the spectral-domain method is well known [4], [5] and the derivation of the Green's function is similar to [2], it will be described only briefly. The discrete Fourier transform of the current densities on the conductors and the electric fields tangent to the surfaces at $z = \pm d_2$ are related by the discrete Fourier transform of the Green's function as follows:

$$\begin{bmatrix} \tilde{E}_x^+(k_{yn}) \\ \tilde{E}_x^-(k_{yn}) \\ \tilde{E}_y^+(k_{yn}) \\ \tilde{E}_y^-(k_{yn}) \end{bmatrix} = \begin{bmatrix} Q_{xx}^{++}(-\beta,k_{yn}) & Q_{xx}^{+-}(-\beta,k_{yn}) & Q_{xy}^{++}(-\beta,k_{yn}) & Q_{xy}^{+-}(-\beta,k_{yn}) \\ Q_{xx}^{-+}(-\beta,k_{yn}) & Q_{xx}^{--}(-\beta,k_{yn}) & Q_{xy}^{-+}(-\beta,k_{yn}) & Q_{xy}^{--}(-\beta,k_{yn}) \\ Q_{yx}^{++}(-\beta,k_{yn}) & Q_{yx}^{+-}(-\beta,k_{yn}) & Q_{yy}^{++}(-\beta,k_{yn}) & Q_{yy}^{+-}(-\beta,k_{yn}) \\ Q_{yx}^{-+}(-\beta,k_{yn}) & Q_{yx}^{--}(-\beta,k_{yn}) & Q_{yy}^{-+}(-\beta,k_{yn}) & Q_{yy}^{--}(-\beta,k_{yn}) \end{bmatrix} \begin{bmatrix} \tilde{J}_x^+(k_{yn}) \\ \tilde{J}_x^-(k_{yn}) \\ \tilde{J}_y^+(k_{yn}) \\ \tilde{J}_y^-(k_{yn}) \end{bmatrix} \quad (5)$$

where the $\pm$ signs refer to the surfaces $z = \pm d_2$. The discrete Fourier transform is defined by

$$\tilde{F}(k_{yn}) = \int_{-a/2}^{a/2} F(y) e^{-jk_{yn}y}\, dy \tag{6a}$$

$$F(y) = \frac{1}{a} \sum_{n=-\infty}^{\infty} \tilde{F}(k_{yn}) e^{jk_{yn}y} \tag{6b}$$

$$k_{yn} = \frac{n\pi}{a}. \tag{6c}$$

The longitudinal currents are assumed to be symmetric around $y = 0$ and the transverse currents are antisymmetric. In order for the fields to have the proper behavior at the sidewalls and due to the symmetries in the assumed currents, n takes on only odd values. The derivation of the Green's function in (5) is outlined in Appendix I.

The strip current densities are expanded in terms of known basis functions f_{xl} and f_{yl} such that

$$\tilde{J}_i^j(k_{yn}) = \sum_{l=1}^{N_{ij}} A_{il}^j \tilde{f}_{il}^j(k_{yn}), \qquad i = x \text{ or } y \text{ and } j = + \text{ or } - \tag{7}$$

where A_{il}^j are unknown constants, the index i refers to direction, the index j refers to surface, and the index l refers to the order of the expansion function. Applying Galerkin's method along with Parseval's theorem, we obtain a set of algebraic equations for the unknown coefficients A_{il}^j. A typical matrix element is described by

$$(Z_{yx}^{+-})_{lp} = \sum_{n=-\infty}^{\infty} \tilde{f}_{yl}^{+}(-k_{yn}) Q_{yx}^{+-}(-\beta, k_{yn}) \tilde{f}_{xp}^{-}(k_{yn}). \tag{8}$$

The values of β which make the determinant of the characteristic matrix equal to zero are the propagation constants for the c and π modes. The following functions have been chosen for $f_{il}^j(y)$:

$$f_{xl}^j(y) = \frac{\cos l\pi(y'/S_k + 0.5)}{\sqrt{(S_k/2)^2 - (y')^2}} \tag{9}$$

$$f_{yl}^j(y) = \frac{\sin l\pi(y'/S_k + 0.5)}{\sqrt{(S_k/2)^2 - (y')^2}} \tag{10}$$

$$y' = y - y_k$$

where S_k is the strip width and y_k is the center of the kth strip (k depends on j).

Once the propagation constant and expansion coefficients are determined for each mode, the ratios $K_c \equiv I_{c1}/I_{c2}$ and $K_\pi \equiv I_{\pi 1}/I_{\pi 2}$ can be determined, where I_{c1}, I_{c2}, $I_{\pi 1}$, and $I_{\pi 2}$ are the total *longitudinal* current on the appropriate center conductor for the appropriate mode. In addition, the power flow for each mode can be calculated according to

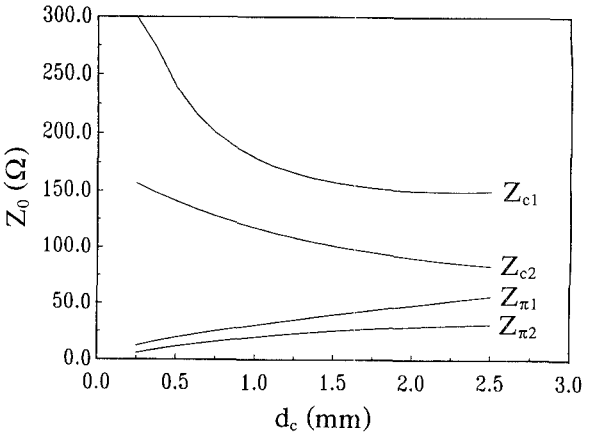

Fig. 4. Typical computed (a) impedance and (b) effective permittivity for a single substrate transition with dimensions of $W_m = 1.15$ mm, $S_1 = 2.0$ mm, $S_1 + 2W = 6.0$ mm, $S_2 = 12.0$ mm, $d_c = 1.27$ mm, and $F = 4.5$ GHz.

$$P_{c,\pi} = \frac{1}{2} \mathrm{Re}\left[\iint (E_y H_z^* - E_z H_y^*)_{c,\pi}\, dy\, dz\right]. \tag{11}$$

These quantities are then used in the definition of the full-wave c and π impedances.

In order to ensure power conservation, Z_{c1}, Z_{c2}, $Z_{\pi 1}$, and $Z_{\pi 2}$ are constrained to satisfy

$$P_c = \frac{1}{2} Z_{c1} |I_{c1}|^2 + \frac{1}{2} Z_{c2} |I_{c2}|^2 = \frac{1}{2} \left(Z_{c1} + Z_{c2}/K_c^2\right) |I_{c1}|^2 \tag{12}$$

$$P_\pi = \frac{1}{2} Z_{\pi 1} |I_{\pi 1}|^2 + \frac{1}{2} Z_{\pi 2} |I_{\pi 2}|^2 = \frac{1}{2} \left(Z_{\pi 1} + Z_{\pi 2}/K_\pi^2\right) |I_{\pi 1}|^2. \tag{13}$$

Two further constraints are necessary for a unique definition of the four impedances. In the low-frequency limit, the impedances should revert to their quasi-static values. To ensure that this happens, equations (4) are imposed as constraints. Combining (4), (12), and (13) yields the fol-

lowing expressions:

$$Z_{c1} = \frac{2P_c}{(1 - K_\pi/K_c)|I_{c1}|^2} \tag{14}$$

$$Z_{\pi 1} = \frac{2/P_\pi}{(1 - K_c/K_\pi)I_{\pi 1}|^2} \tag{15}$$

with Z_{c2} and $Z_{\pi 2}$ determined from (4).

Fig. 4 shows representative impedance and propagation constants for a set of coupled lines which could form a transition from one side of a substrate to the other (no motherboard). Referring to Fig. 3, $\{\epsilon_1, \epsilon_3, \epsilon_4\}$ are set to one and $\{d_1, d_4\}$ are made large. Fig. 4 shows the resulting impedance values versus substrate thickness, d_c. Note that as substrate thickness increases the c and π mode impedances move toward each other, indicating lower coupling.

III. Results

In this section experimental results are presented for two couplers which have been designed using the previously described analysis. At present, there is no definitive design method. A particular set of substrate characteristics and frequency is defined by the application. A trial size $S_1 + 2W$ is then chosen and fixed while W and W_m are varied. Each set of values results in a set comprising Z_{c1}, Z_{c2}, $Z_{\pi 1}$, $Z_{\pi 2}$, β_c, and β_π, which are then combined with equations (1) to describe the two-port. A possible design is achieved when a 50 Ω impedance is seen at the input while the output is terminated in 50 Ω. If no design is achieved, $S_1 + 2W$ is increased and W and W_m are again varied and so on. The coupler length is initially set at a quarter of the average of the mode wavelengths and later adjusted for best bandwidth and match. The width of the CPW ground plane, S_2, is made large enough that the coupler response is independent of it.

A. Single-Substrate Transition

A single transition was constructed between CPW and microstrip on opposite sides of a single substrate (Duroid 6010.2, 1.27 mm thick, $\epsilon_r = 10.2$). No motherboard was involved in this case. The dimensions of the coupler (see Fig. 3) are as follows: $W_m = 1.15$ mm, $S_1 = 2.0$ mm, $S_1 + 2W = 6.0$ mm, $d_c = 1.27$ mm; the length of the coupled region, L, is 7.0 mm and the gap size, g, is 1.0 mm. Measured return loss, shown in Fig. 5, is better than 20 dB over a 35 percent bandwidth. This measurement is of the coupler de-embedded from its two coax transitions using the time-domain option on an HP-8510 network analyzer. The measured insertion loss (including coax transitions) is about 0.7 dB in the passband. Also shown in Fig. 5 is the return loss predicted using a full-wave and quasi-static analysis. The quasi-static analysis was performed for comparison and is described in Appendix II. Both methods show good agreement with the measured results.

Two more single-substrate transitions were designed for operation at 10 GHz. Both were built on Duroid 6010.2. The first had dimensions of $W_m = 1.3$ mm, $S_1 + 2W = 7.0$ mm, $S_1 = 1.25$ mm, $d_c = 1.27$ mm, and $L = 3.0$ mm. Poor agreement between theory and measurement was observed. This is likely to be due to the small ratio of length to width in this design (see Section IV). The second design had dimensions of $W_m = 0.6$ mm, $S_1 + 2W = 3.0$ mm, $S_1 = 0.4$ mm, $d_c = 0.635$ mm, $L = 3.0$ mm, and $g = 0.3$ mm. Measurements of this transition showed a return loss of better than 20 dB over a 49 percent bandwidth and were in good agreement with theory except for a center frequency which was observed to be 8 percent lower than predicted.

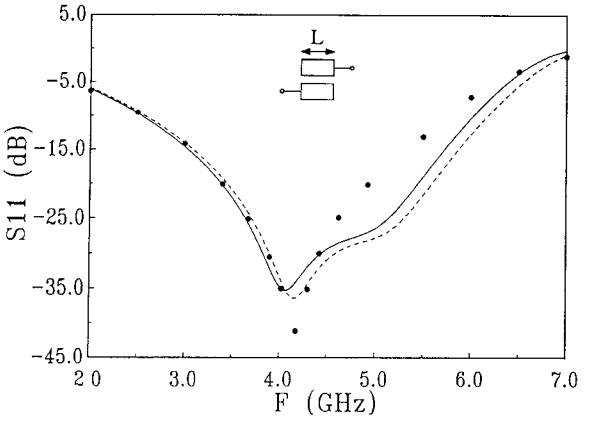

Fig. 5. Measured $|S_{11}|$ for the single substrate transition (●●●), full-wave (——), and quasi-static (– – – –).

It should be noted that there is a degree of freedom in choosing the size of the gap which forms the open end of the CPW part of the coupler. For the single-substrate coupler, a gap size of roughly 10 percent of the total length has been found to give the best results in terms of bandwidth and match. It has also been determined (empirically) that the microstrip part of the coupler should extend over the entire length of the coupler including the gap.

The coupled transmission line model (see inset to Fig. 5) agrees best with measured results if the model coupling length is defined to be the length of the CPW center conductor plus the size of the gap. The coupler described in the next section requires a more complicated model.

B. Chip to Motherboard Transition

Fig. 6 shows the dimensions for a two-transition microstrip to CPW coupler (again, using Duroid 6010.2 substrates). The first transition is from a CPW motherboard ($d_m = d_3 = 0.635$ mm) to a microstrip chip ($d_c = 2d_2 = 0.635$ mm) and the second returns the signal to the CPW motherboard. The measured return loss of the two transitions combined is shown in Fig. 7 and is better than 15 dB over a 47 percent bandwidth. Again, the transitions were de-embedded from the coax connectors. The insertion loss of the entire structure (including coax to CPW transitions) is about 1.7 dB. Fig. 7 compares the measured return loss to the predicted return loss using the full-wave analysis. Good agreement with the measured return loss is apparent over most of the band. A quasi-static analysis of this structure (not shown) agrees with the full-wave results at low frequencies, but above 7 GHz they disagree signifi-

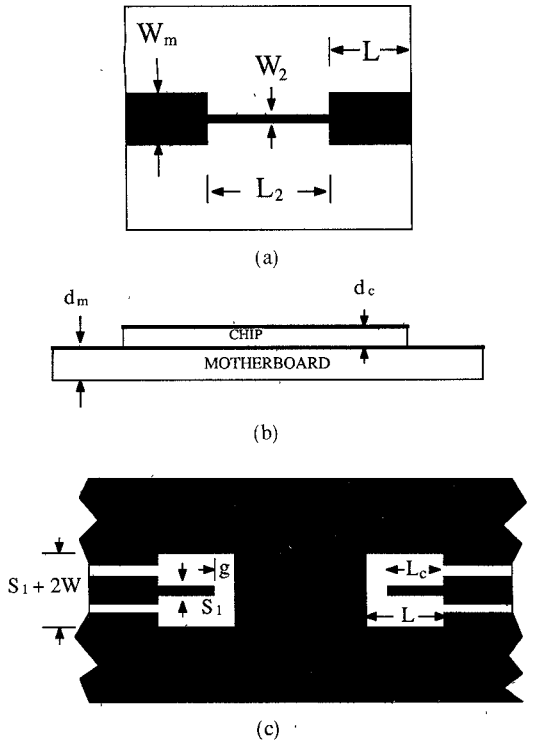

Fig. 6. Test configuration: (a) top view of chip, (b) cross section, and (c) top view of motherboard with dimensions of $W_m = 2.0$ mm, $S_1 = 0.75$ mm, $S_1 + 2W = 5.0$ mm, $L = 4.5$ mm, $L_c = 3.5$ mm, $g = 1.0$ mm, $d_m = d_c = 0.635$ mm, $W_2 = 0.56$ mm, and $L_2 = 17.0$ mm.

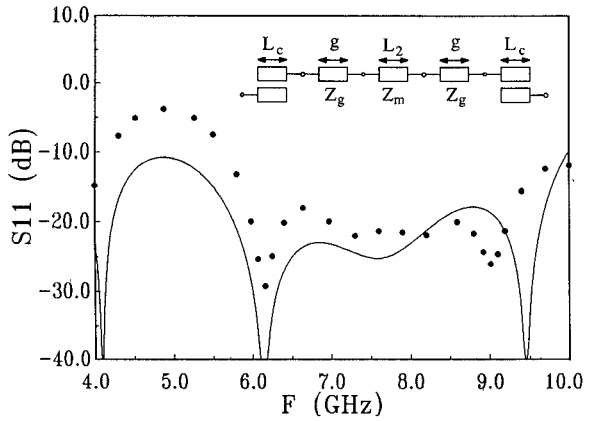

Fig. 7. Measured (●●●) and predicted (——) $|S_{11}|$ for the test configuration in Fig. 6.

cantly. This can be attributed to the presence of the high permittivity (10.2) motherboard, which causes greater dispersion than might be encountered in a single-substrate coupler.

As in the single-substrate coupler, the best choice of gap width was determined empirically. In this case, it amounted to about 20 percent of the total transition length.

Modeling this structure is slightly more complicated than modeling the single-substrate transition. The best agreement between theory and measurement is obtained if the physical transition is modeled by an ideal coupler of length L_c followed by a short piece of transmission line of length g (see inset to Fig. 7) which models the effect of the discontinuity over the gap. The impedance and electrical length of this last piece of line are obtained by analyzing Fig. 3 with the center CPW strip (width S_1) removed.

IV. Discussion

In modeling these transitions using a coupled transition line analysis, it is assumed that the discontinuity effects do not dominate the structures' electromagnetic behavior. This suggests that the length (L) to width ($S_1 + 2W$) ratio should be large for proper agreement between theory and experiment. The transitions described in Section III have length to width ratios of 1.2, 0.45, 1.0, and 0.9, respectively. Only the second one showed a poor agreement with theory. We have also fabricated a transition with a length to width ratio of 0.6 and obtained good agreement with theory except at the high end of the band.

In order to determine the suitability of this transition for millimeter integrated circuit applications, several paper designs have been completed. A 35 GHz transition from a 0.127 mm alumina motherboard to a 0.1 mm GaAs chip is computed to have the following dimensions (see Fig. 3): $S_1 = 150$ μm, $S_1 + 2W = 1000$ μm, $W_m = 400$ μm, and $L = 880$ μm. A 0.254 mm quartz motherboard was also considered. This transition is computed to have the following dimensions: $S_1 = 100$ μm, $S_1 + 2W = 700$ μm, $W_m = 240$ μm, and $L = 990$ μm. The size of the new transition is too large for use in current MMIC circuits (1 mm × 2 mm) but may have applications in larger IC's which will be used in the future [1].

V. Conclusions

A transition has been developed for coupling a microstrip line on one surface to coplanar waveguide on another. Asymmetric coupled line theory and a full-wave analysis were used to predict the behavior of this transition. Measured results show reasonably good agreement with theory as long as the transition length is sufficiently long in comparison to its width.

This transition is likely to have applications in large integrated or hybrid circuits where wire bonds are undesirable.

Appendix I

The fields in each layer of Fig. 3 can be obtained from the z-directed magnetic and electric potentials in each of the four layers by

$$\begin{aligned}
\tilde{\psi}_1^m &= C_1^m \cos k_1(d_1 + d_2 - z) \\
\tilde{\psi}_2^e &= C_1^e \sin k_1(d_1 + d_2 - z) \\
\tilde{\psi}_2^m &= C_2^m \cos k_2 z + D_2^m \sin k_2 z \\
\tilde{\psi}_2^e &= C_2^e \cos k_2 z + D_2^e \sin k_2 z \\
\tilde{\psi}_3^m &= C_3^m \cos k_3(d_2 + z) + D_3^m \sin k_3(d_2 + z) \\
\tilde{\psi}_3^e &= C_3^e \cos k_3(d_2 + z) + D_3^e \sin k_3(d_2 + z) \\
\tilde{\psi}_4^m &= C_4^m \cos k_4(d_2 + d_3 + d_4 + z) \\
\tilde{\psi}_4^e &= C_4^e \sin k_4(d_2 + d_3 + d_4 + z).
\end{aligned} \tag{A1}$$

Here $k_i = (\epsilon_i k_0^2 - k_x^2 - k_y^2)^{1/2}$, the subscripts $i = 1, 2, 3, 4$ refer to the different layers, and

$$C_2^m = C_{21}^m + C_{22}^m$$

$$C_{21}^m = \frac{j(k_1/\epsilon_1)\left(k_x \tilde{J}_{x1} + k_y \tilde{J}_{y1}\right)}{k_x^2 + k_y^2} \cdot \frac{TM_4 \sin k_1 d_1}{DM}$$

$$C_{22}^m = \frac{-j(k_3/\epsilon_3)\left(k_x \tilde{J}_{x2} + k_y \tilde{J}_{y2}\right)}{k_x^2 + k_y^2} \cdot \frac{TM_2 TM_5}{DM}$$

$$C_2^e = C_{21}^e + C_{22}^e$$

$$C_{21}^e = \frac{\eta_0 k_0\left(k_y \tilde{J}_{x1} - k_x \tilde{J}_{y1}\right)}{k_x^2 + k_y^2} \cdot \frac{TE_4 \sin k_1 d_1}{DE}$$

$$C_{22}^e = \frac{\eta_0 k_0\left(k_y \tilde{J}_{x2} - k_x \tilde{J}_{y2}\right)}{k_x^2 + k_y^2} \cdot \frac{TE_2 TE_6}{DE}$$

$$D_2^m = \left(-\frac{TM_3}{TM_4} C_{21}^m + \frac{TM_1}{TM_2} C_{22}^m\right)$$

$$D_2^e = \left(\frac{TE_3}{TE_4} C_{21}^e - \frac{TE_1}{TE_2} C_{22}^e\right)$$

$$C_1^m = \left(\frac{\epsilon_1 k_2}{\epsilon_2 k_1}\right)\left(-C_2^m \sin k_2 d_2 + D_2^m \cos k_2 d_2\right)/\sin k_1 d_1$$

$$C_1^e = \left(C_2^e \cos k_2 d_2 + D_2^e \sin k_2 d_2\right)/\sin k_1 d_1$$

$$C_3^e = C_2^e \cos k_2 d_2 - D_2^e \sin k_2 d_2$$

$$D_3^m = \frac{\epsilon_3 k_2}{\epsilon_2 k_3}\left(C_2^m \sin k_2 d_2 + D_2^m \cos k_2 d_2\right)$$

$$D_3^e = \frac{TE_5}{TE_6} C_3^e \qquad C_3^m = -\frac{TM_6}{TM_5} D_3^m$$

$$C_4^e = \left(C_3^e \cos k_3 d_3 - D_3^e \sin k_3 d_3\right)/\sin k_4 d_4$$

$$C_4^m = -\frac{\epsilon_4 k_3}{\epsilon_3 k_4}\left(C_3^m \sin k_3 d_3 + D_3^m \cos k_3 d_3\right)/\sin k_4 d_4$$

$$TM_1 = \left(\frac{k_2}{\epsilon_2}\right)\cos k_1 d_1 \sin k_2 d_2 + \left(\frac{k_1}{\epsilon_1}\right)\sin k_1 d_1 \cos k_2 d_2$$

$$TM_2 = \left(\frac{k_2}{\epsilon_2}\right)\cos k_1 d_1 \cos k_2 d_2 - \left(\frac{k_1}{\epsilon_1}\right)\sin k_1 d_1 \sin k_2 d_2$$

$$TM_3 = \left(\frac{k_2}{\epsilon_2}\right)\sin k_2 d_2 TM_6 + \left(\frac{k_3}{\epsilon_3}\right)\cos k_2 d_2 TM_5$$

$$TM_4 = \left(\frac{k_2}{\epsilon_2}\right)\cos k_2 d_2 TM_6 - \left(\frac{k_3}{\epsilon_3}\right)\sin k_2 d_2 TM_5$$

$$TM_5 = \left(\frac{k_3}{\epsilon_3}\right)\sin k_3 d_3 \cos k_4 d_4 + \left(\frac{k_4}{\epsilon_4}\right)\cos k_3 d_3 \sin k_4 d_4$$

$$TM_6 = \left(\frac{k_3}{\epsilon_3}\right)\cos k_3 d_3 \cos k_4 d_4 - \left(\frac{k_4}{\epsilon_4}\right)\sin k_3 d_3 \sin k_4 d_4$$

$$TE_1 = k_1 \cos k_1 d_1 \cos k_2 d_2 - k_2 \sin k_1 d_1 \sin k_2 d_2$$

$$TE_2 = k_1 \cos k_1 d_1 \sin k_2 d_2 + k_2 \sin k_1 d_1 \cos k_2 d_2$$

$$TE_3 = k_3 \cos k_2 d_2 TE_5 - k_2 \sin k_2 d_2 TE_6$$

$$TE_4 = k_3 \sin k_2 d_2 TE_5 + k_2 \cos k_2 d_2 TE_6$$

$$TE_5 = k_4 \cos k_3 d_3 \cos k_4 d_4 - k_3 \sin k_3 d_3 \sin k_4 d_4$$

$$TE_6 = k_4 \sin k_3 d_3 \cos k_4 d_4 + k_3 \cos k_3 d_3 \sin k_4 d_4$$

$$DM = TM_1 TM_4 + TM_2 TM_3$$

$$DE = TE_1 TE_4 + TE_2 TE_3. \tag{A2}$$

The Fourier series amplitudes are then obtained from

$$\tilde{\vec{E}}_i = -\tilde{\vec{\nabla}} \times \tilde{\psi}_i^e \hat{z} + \frac{1}{j\omega\epsilon_0\epsilon_i} \tilde{\vec{\nabla}} \times \tilde{\vec{\nabla}} \times \tilde{\psi}_i^m \hat{z}$$

$$\tilde{\vec{H}}_i = \tilde{\vec{\nabla}} \times \tilde{\psi}_i^m \hat{z} + \frac{1}{j\omega\mu_0} \tilde{\vec{\nabla}} \times \tilde{\vec{\nabla}} \times \tilde{\psi}_i^e \hat{z}$$

where

$$\tilde{\vec{\nabla}} = jk_x \hat{x} + jk_y \hat{y} + \hat{z} \frac{\partial}{\partial z}.$$

Appendix II
Quasi-Static Analysis

The discrete Fourier transform of the charge densities on the conductors in Fig. 2 and the potential at the surfaces $z = \pm d_2$ are related to the Fourier transform of the quasi-static Green's function [6] as follows:

$$\begin{bmatrix} \tilde{\phi}(k_{yn}, d_2) \\ \tilde{\phi}(k_{yn}, -d_2) \end{bmatrix} = \begin{bmatrix} G_{11}(k_{yn}) & G_{12}(k_{yn}) \\ G_{21}(k_{yn}) & G_{22}(k_{yn}) \end{bmatrix} \begin{bmatrix} \tilde{\rho}_1(k_{yn}) \\ \tilde{\rho}_2(k_{yn}) \end{bmatrix} \tag{A3}$$

where ρ_1 is the charge density on the microstrip line, and ρ_2 is the charge density on the CPW. The charge density is expanded into a series of the form

$$\tilde{\rho}_i(k_{yn}) = \sum_{l=1}^{N_i} B_{il} \tilde{f}_{il}(k_{yn}), \qquad i = 1 \text{ or } 2 \tag{A4}$$

where $\tilde{f}_{il}(k_{yn})$ are the Fourier transform of known functions (eq. (9)), B_{il} are unknown coefficients, and the index $i = 1$ or 2 refers to the surfaces at $z = d_2$ and $-d_2$, respectively.

The standard Galerkin procedure is then applied in order to obtain the unknown B_{il} in terms of given potentials on each of the lines. A capacitance matrix results which is then used to determine β_c, β_π, Z_{c1}, Z_{c2}, $Z_{\pi 1}$, and $Z_{\pi 2}$ in a manner similar to that in [3].

References

[1] J. A. Kinzel, "GaAs technology for millimeter phased arrays," *IEEE Antennas Propagat. Newsletter*, vol. 29, pp. 12–14, Feb. 1987.

[2] R. W. Jackson and D. W. Matolak, "Surface-to-surface transition via electromagnetic coupling of coplanar waveguides," *IEEE Trans. Microwave Theory Tech.*, vol. MTT-35, pp. 1027–1032, Nov. 1987

[3] V. K. Tripathi, "Asymmetric coupled transmission lines in an inhomogeneous medium," *IEEE Trans. Microwave Theory Tech.*, vol. MTT-23, pp. 734–739, Sept. 1975.

[4] R. Jansen, "Unified user oriented computation of shielded, covered and open planar microwave and millimeter wave transmission line characteristics," *Microwave, Opt. Acoustic*, vol. 3, pp. 14–22, Jan. 1979.

[5] T. Itoh, "Spectral-domain immittance approach for dispersion characteristics of generalized printed transmission lines," *IEEE Trans. Microwave Theory Tech.*, vol. MTT-28, pp. 733–736, July 1980.

[6] K. C. Gupta *et al.*, *Microstrip Line and Slotlines*. Dedham, MA: Artech House, 1979, p. 20.

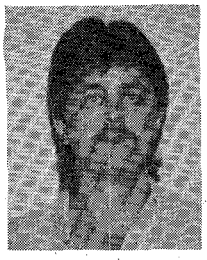

John J. Burke (S'83) was born in Elizabeth, NJ, on June 9, 1962. He received the B.S.E.E. degree from Northeastern University, Boston, MA, in 1984 and the M.S.E.E. degree from the University of California at Los Angeles in 1986. He is currently studying at the University of Massachusetts for the Ph.D. degree.

From 1984 to 1986, he was with the Space and Communications Group, Hughes Aircraft, El Segundo, CA. In 1987 he joined the Microwave Electronics Laboratory at the University of Massachusetts. His research interests include the computer-aided analysis and design of microwave circuitry.

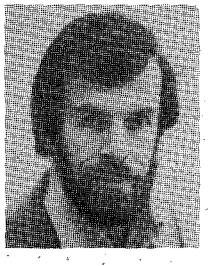

Robert W. Jackson (M'82–SM'88) was born in Boston, MA, on October 18, 1952. He received the B.S. (1975) and Ph.D. (1981) degrees in electrical engineering from Northeastern University, Boston, MA. His thesis was on nonlinear plasma interactions in the earth's bow shock.

From 1981 to 1982 he was an Assistant Professor at Northeastern University. Since 1982, he has been on the faculty of the Department of Electrical and Computer Engineering at the University of Massachusetts, Amherst, where he is a member of the Microwave and Electronics Laboratory. His research interests include numerical electromagnetics applied to millimeter-wave integrated circuits and active microwave and millimeter-wave circuit design.